Chemical Physics xxx (xxxx) 112063

Contents lists available at ScienceDirect

Chemical Physics

journal homepage: www.elsevier.com/locate/chemphys

Crystal polymorphs and molecular conformations of fluorinated ionic liquid: 1-Ethyl-3-methylimidazolium perfluorobutanesulfonate

Hiroshi Abe [a,*], Hiroaki Kishimura [a], Mikio Uruichi [b], Hajime Sagayama [c]

[a] Department of Materials Science and Engineering, National Defense Academy, Yokosuka 239-8686, Japan
[b] Institute for Molecular Science, Myodaiji, Okazaki 444-8585, Japan
[c] Institute of Materials Structure Science, High Energy Accelerator Research Organization (KEK), Tsukuba 305-0801, Japan

ARTICLE INFO

Keywords:
Fluorinated ionic liquid
Molecular conformations
Crystal polymorph
Phase transition

ABSTRACT

The phase transitions of a fluorinated ionic liquid (fIL) were examined at low temperature (LT) by X-ray diffraction and Raman spectroscopy. The fIL was 1-ethyl-3-methylimidazolium perfluorobutanesulfonate ([C_2mim][PFBS]). The cation and anion possessed conformational degrees of freedom. The *trans* and *gauche* conformers of $[PFBS]^-$ coexisted in the liquid state. The LT crystal polymorph of the [C_2mim][PFBS] was observed, and [C_2mim][PFBS] possessed the large unit cells. The *gauche*' conformer of $[PFBS]^-$ appeared, accompanying with the phase transition at 220 K.

1. Introduction

Amorphous compounds, crystals, or their combinations in a molecular system are selected mainly by their molecular conformations. Amorphous and supercooled liquids are analyzed using a free energy landscape (FEL) [1]. In crystals, large unit cells, including lattice modulations, are induced by a variety of molecular conformations. The number of molecules in the unit cell, *Z*, is governed by the conformational degrees of freedom [2]. Moreover, crystal polymorphs with changing molecular conformations and packing are observed at temperature and pressure scales [3]. The computer-aided predictions of crystal structures have been highlighted for the last two decades [4,5]. To describe the crystal polymorphs in molecular systems, the crystal energy landscape (CEL) was established by applying the concept of the FEL. The crystal structure predictions are significant for pharmaceutical polymorph screening [6]. The physicochemical properties of pharmaceutical compounds are easily modified using crystal polymorphs. Thus, crystal polymorph screening is important in the pharmaceutical industry.

Various scientific fields have been interested in ionic liquids (ILs). The unique properties and applications of the ILs are summarized in the literature [7,8]. The glass transition and crystallization temperatures of the ILs are obtained systematically [8]. Furthermore, the crystal polymorphs and multiple crystallization pathways in the ILs are clarified at low temperature (LT) and high pressure (HP) [9–11]. The CEL supports the complicated phase behaviors of the ILs, depending on the cooling rate. The crystal polymorphs and multiple crystallization pathways of the ILs are regarded as non-equilibrium phenomena. Using the 1-alkyl-3-methylimidazolium cations, $[C_n\text{mim}]^+$, the anion effects in the solid states are examined [12], where *n* is the alkyl chain length of the cation. In [C_6mim][X], the anionic size effects on solidifications are observed, where X is an anion. In [C_2mim]-based ILs, the crystal structures are determined at room temperature [13]. The anion effect in the crystal is clarified in the unit cells. More importantly, for [C_2mim][NO_3], the HP-inherent molecular conformer of $[C_2\text{mim}]^+$ results in HP multiple crystallization pathways and HP crystal polymorphs [14]. The large unit cells under HP imply that the modulated lattice is induced by high molecular packing. Further, for the crystal structures of [C_2mim][X], the LT phase behaviors and heat capacities are examined at ambient pressure [15,16]. The perfluorobutanesulfonate anion ($[PFBS]^-$) as a fluorinated IL (fIL) has two stable conformations: *trans* (t) and *gauche* (g) [17]. In the LT crystal of [C_4mim][PFBS], the t conformer of the $[PFBS]^-$ is preferred. Despite the simple molecular structure of the $[C_2\text{mim}]^+$, crystal polymorphs appear under HP in the [C_2mim][Cl] system [18]. The complicated phase transitions in the [C_2mim][Cl] are induced by the molecular conformational changes of $[C_2\text{mim}]^+$. The HP crystal polymorphs of the [C_4mim][PFBS] [19] and [C_6mim][PFBS] [20] are observed by X-ray diffraction and Raman spectroscopy. The crystal polymorphs are attributed to the molecular conformations of the cation and anion.

In this study, we investigate the relationship between the conformers and crystal structures of the [C_2mim][PFBS] at LT. A variety of LT

* Corresponding author.
E-mail address: ab@nda.ac.jp (H. Abe).

https://doi.org/10.1016/j.chemphys.2023.112063
Received 12 June 2023; Received in revised form 11 August 2023; Accepted 23 August 2023
0301-0104/

phases of a simple molecular system is derived from the conformational degrees of freedom of the cation and anion.

2. Experiments

The [C_2mim][PFBS] IL used in this study was provided by GS Alliance Co. The [C_2mim]$^+$ cation possesses three kinds of conformer: *planar* (P), *non-planar* (NP), and *planar'* (P') [21], and the t, g [17], and *gauche'* (g') [22] of [PFBS]$^-$ are depicted in Fig. 1.

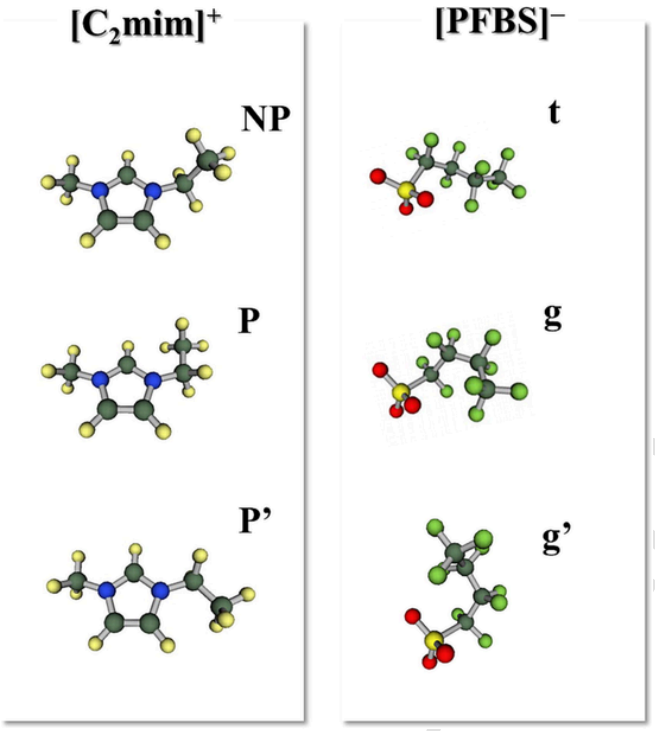

Fig. 1. Molecular conformations of the [C_2mim]$^+$ cation and [PFBS]$^-$ anion. NP, P, and P' are the *non-planar*, *planar*, and *planar'* conformations of the [C_2mim]$^+$, respectively. The [PFBS]$^-$ conformers are *trans* (t), *gauche* (g), and *gauche'* (g').

To determine the LT phases, simultaneous X-ray diffraction and differential scanning calorimetry (DSC) measurements were performed using SmartLab (Rigaku Co.) [23]. The wavelength of incident X-ray (Cu radiation) was selected as $\lambda = 0.1542$ nm with 2θ as the scattering angle. The wave vector, Q, was $4\pi (\sin\theta)/\lambda$. The cooling and heating rate was 2 K/min.

Powder X-ray diffraction using a high-speed spinner was performed to remove the typical preferred orientation of the Debye rings on the BL-8B beamline of the Photon Factory at the High-Energy Accelerator Research Organization (KEK) in Japan. Two-dimensional diffraction patterns were obtained using a cylindrical imaging plate system (R-AXIS, Rigaku Co.). The liquid sample was put into the quartz capillary, whose diameter was 0.3 mm. The cooling system used was GN2-SN (Rigaku Co.), with heating rate of 2 K/min. The incident wavelength ($\lambda = 0.09957$ nm) was calibrated using a CeO_2 polycrystalline standard. *Conograph* [24] and *FOX* [25] were used to analyze the crystal structures. *Conograph* was used to calculate the possible lattice parameters and space groups, and *FOX* was used to identify the space groups through global optimization.

Raman spectra were measured using a Via Reflex (RENISHAW). A 785 nm semiconductor laser was used as an excitation source with a power of 0.35 mW, A helium flow cryostat (Microstat He, Oxford) was installed to cool samples. In the thermal cycle, the cooling and heating rate was not constant. The Raman spectra were collected at fixed temperatures. The resolution of the Raman spectroscopy was 1 cm^{-1}.

3. Results and discussion

3.1. Crystal polymorphs of the 1-ethyl-3-methylimidazolium perfluorobutanesulfonate by simultaneous measurements

The phase behaviors of the [C_2mim][PFBS] were examined using simultaneous X-ray diffraction and DSC measurements. A LT crystal polymorph was observed in [C_2mim][PFBS] (Fig. 2). Upon cooling, crystallization occurred at 276 K (T_{C1}) with an exothermal peak and sharp Bragg peaks, herein, referred to as the C_I phase. Subsequently, a small exothermal peak appeared at 274 K (T_{C2}), which is the C_{II} phase, i.e., the phase transition at T_{C2}, as shown in Fig. 2. Since T_{C2} was close to T_{C1}, the crystal structure of the C_I phase was not distinguished from that of the C_{II} phase. By further cooling, the additional phase transition was probed on the DSC thermal trace. At 202 K (T_{C3}), a weak exothermal

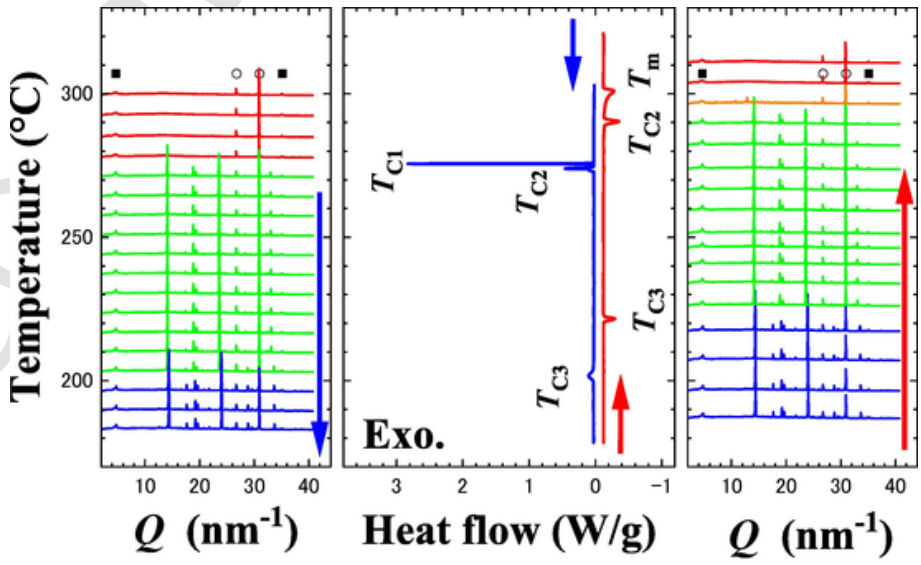

Fig. 2. X-ray diffraction patterns and DSC thermal traces of the [C_2mim][PFBS]. T_{C1}, T_{C2}, and T_{C3} are the phase transition temperatures. T_m is the melting point upon heating. Open circles indicate the Bragg reflections from an Al sample pan, whereas the additional scattering from the DSC inner shroud is shown by the green closed square.

peak was obtained, accompanied by additional weak Bragg reflections, as observed in the X-ray diffraction pattern (Fig. 2). The C_{III} phase appeared below T_{C3}, although the difference between the C_{II} and C_{III} phases was small. The minimum temperature (T_{min}) in the simultaneous measurements of X-ray diffraction and DSC was 173 K.

In the ILs, reversible or irreversible crystal polymorphs were classified in the thermal cycle. In the [$C_n$mim][PFBS] (n = 4, 6, and 8), the irreversible crystal polymorphs were obtained at LT [17]. Upon heating (Fig. 2), in the [C_2mim][PFBS], the endothermal peak was detected at 221 K (T_{C3}). Judging from the X-ray diffraction pattern, the C_{III}–C_{II} phase transition occurred reversely with disappearing weak Bragg reflections, and the hysteresis was small (ΔT_{III} = 19 K). With the increase in temperature, T_{C2} was observed at 290 K (Fig. 2). Considering the temperature region of the C_{II} phase upon cooling and heating, the hysteresis (ΔT_{II}) was 16 K. Above T_{C2}, the X-ray diffraction pattern, as revealed by the orange curve in Fig. 2, is different from that of the C_{II} phase. Thus, we deduce that the C_{II} phase transformed to the C_I phase at 290 K. When the C_{II}–C_I phase transition occurred reversely upon heating, the LT crystal polymorph of the [C_2mim][PFBS] exhibited a complete reversible phase transition with a small hysteresis. Finally, the crystal melted at 301 K (T_m) (Fig. 2). In the liquid state, the prepeak representing the nanoheterogeneity did not exist in the [C_2mim][PFBS].

3.2. Crystal polymorphs and conformations of the 1-ethyl-3-methylimidazolium perfluorobutanesulfonate by simultaneous measurements

The conformations of the [$C_n$mim][PFBS] (n = 4, 6, and 8) at LT were determined using Raman spectroscopy [26]. The occurrence of different crystal polymorphs is due to the presence of different anion or cation conformers. For the [C_2mim]$^+$, the P' conformer (Fig. 1) was induced under HP. By density functional theory (DFT) [21], the P' conformer was evaluated to be unstable. Moreover, the g' conformer of the [PFBS]$^-$ (Fig. 1) was formed under HP [22].

Fig. 3 indicates the temperature dependence of the Raman spectra of the [C_2mim][PFBS]. Using an optical microscope, it was found that the [C_2mim][PFBS] was in a liquid state at 290 K. The P and NP of the [C_2mim]$^+$ exhibited weak and broad Raman bands. The Raman bands of the [C_2mim][PFBS] coincided with those of the [C_2mim][X] [27]. Additionally, the [PFBS]$^-$ Raman bands of the [C_2mim][PFBS] in the liquid state were comparable to those of the [$C_n$mim][PFBS] (n = 4, 6, and 8) [26]. The time interval between the 290 K and 280 K measurements was 37 min, including the temperature stabilization time. At 280 K, crystal domains were observed using the optical microscope. The crystallization temperature was higher than 276 K (T_{C1}), which was determined by the simultaneous measurements of X-ray diffraction and DSC (Fig. 2). One of the reasons is that the cooling rate of the LT Raman spectroscopy was considerably low. Although the crystalliza-

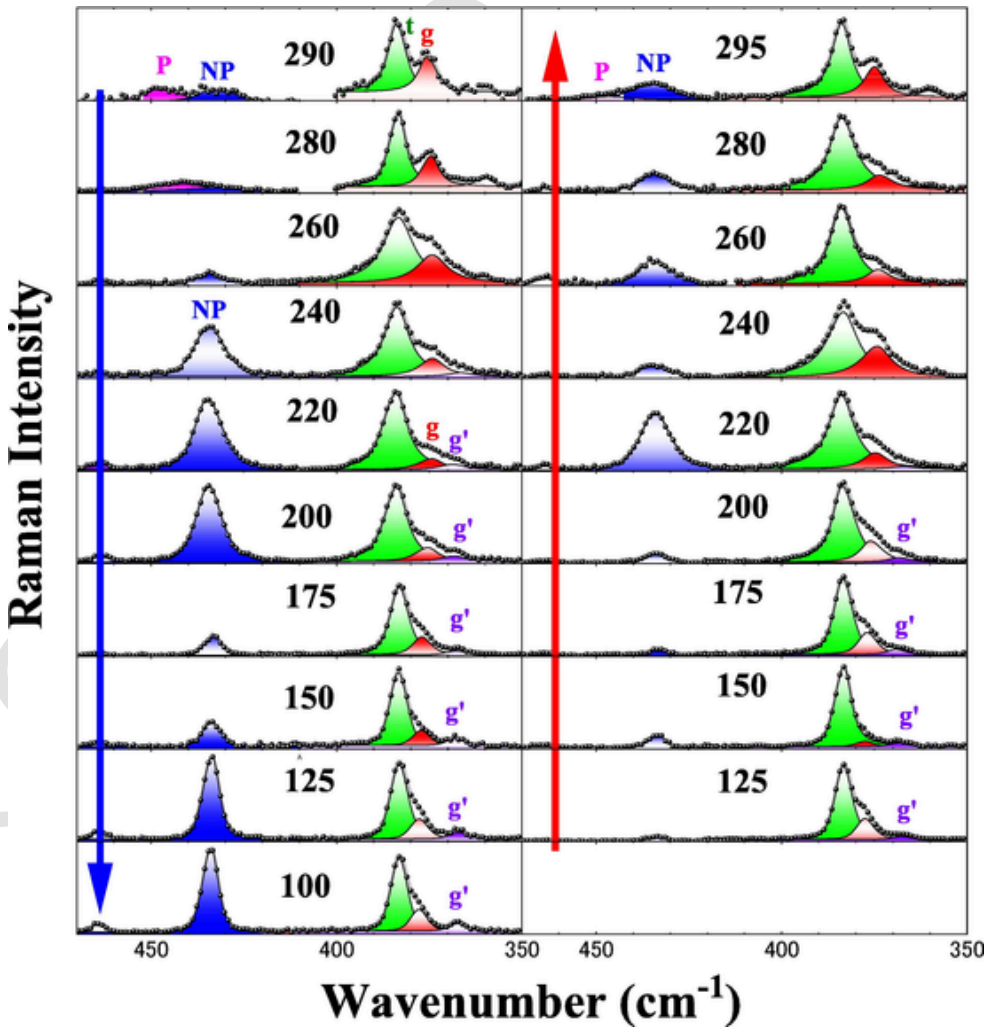

Fig. 3. Temperature dependences of the Raman spectra of the [C_2mim][PFBS] upon cooling and heating. Spectrum changes correspond to the LT crystal polymorph. The numbers in the figure indicate temperatures.

tion occurred, the P and NP Raman bands of the $[C_2mim]^+$ coexisted, and the Raman bands of the $[PFBS]^-$ did not change (Fig. 3). The conformational feature was attributed to the C_I phase. In the crystal state at 260 K, the Raman band of the P of the $[C_2mim]^+$ disappeared completely, and the Raman bands of the $[PFBS]^-$ became relatively broad. Previously, in the unit cells of the $[C_2mim][X]$, the NP conformer of the $[C_2mim]^+$ was formed at LT [28,29]. In contrast, under HP, the crystal consisted only of the P conformer for a relatively high packing efficiency [30]. Hence, the $[C_2mim]^+$ conformers were influenced extensively by the molecular packing circumstances. The drastic changes in the Raman spectra occurred at 240 K. The intensity of the NP Raman bands of the $[C_2mim]^+$ increased, although the g Raman band of the $[PFBS]^-$ decreased. If the Raman spectrum at 240 K was derived from the C_{II} phase, the Raman spectrum at 260 K was a transient state between the C_I and C_{II} phases. Moreover, at 240 K, an additional Raman band of the $[PFBS]^-$ appeared at approximately 367 cm^{-1}. The new band was assigned as the g' conformer using DFT [22]. Since the g' conformer appeared in the well-packed circumstance under HP [22], the C_{III} phase at LT could be a densely packed crystal structure. At 200 K, the Raman spectra did not change distinctly. The C_{II}–C_{III} phase transition upon cooling did not occur at 200 K, although T_{C3} occurred at 202 K, as observed by the simultaneous measurement (Fig. 2). By further cooling, at 175 K, the intensity of the NP Raman band drastically decreased, and the peaks of the $[PFBS]^-$ Raman bands became relatively sharp. Thus, the C_{III} phase was formed below 200 K. The conformational features of the C_{III} phase are observed by the decrease in the NP conformer. This tendency was also seen at 150 K. Nevertheless, at 125 K, the intensity of the NP band increased inversely. The sharp and intense NP band was induced by the C_{III}–C_{IV} phase transition. Since the T_{min} in the simultaneous measurement was 173 K, the C_{IV} phase was not observed. Despite the simple molecular system, the complicated crystal polymorph of the $[C_2mim][PFBS]$ was derived from a variety of the $[C_2mim]^+$ and $[PFBS]^-$ conformers.

Upon heating, the C_{IV} phase transformed to the C_{III} phase at 125 K (Fig. 3). The Raman spectra of the C_{III} phase did not change up to 200 K. At 220 K, a sudden increment in the NP band of the $[C_2mim]^+$ was observed. Additionally, the g' conformer of $[PFBS]^-$ almost vanished, and the broadening of the t and g bands was predominant. Therefore, the reverse C_{III}–C_{II} phase transition occurred at 220 K upon heating. The transition temperature upon heating was comparable to T_{C3} (Fig. 2). With the increase in the temperature, the crystal domains did not vary even at 280 K, as observed using the optical microscope. However, at 295 K, the C_I phase appeared with the P conformer of the $[C_2mim]^+$ (Fig. 3). Additionally, the reversible crystal polymorph of the $[C_2mim][PFBS]$ was confirmed at LT by Raman spectroscopy,

3.3. Crystal structures of the 1-ethyl-3-methylimidazolium perfluorobutanesulfonate

The crystal structures of the $[C_2mim][PFBS]$ were determined by synchrotron radiation experiments using a high-speed spinner. The preferred orientation of the Debye rings was reduced as shown in Fig. S1. Fig. 4 indicates the X-ray diffraction patterns of the $[C_2mim][PFBS]$ upon heating. Here the liquid density, ρ, of the $[C_2mim][PFBS]$ was 1.552 g/cm^3 [31]. By structure analysis, the possible crystal structures of the C_{II} phase at 247 K were found to be, $P2/c$, $P2_1/c$, or $P2/m$. The crystal structure of monoclinic $P2_1/c$ as one of the candidates is presented in Table 1. Despite the simple molecular system, the unit cell of the C_{II} phase was described by the large lattice constants. The molecular arrangements of the $[PFBS]^-$ in the unit cell are illustrated in Fig. 5(a). For simplicity, the $[C_2mim]^+$ cations are omitted. The NP conformers of the $[C_2mim]^+$ were formed in the unit cell. In other systems, such as $[C_2mim][NO_3]$ [14], large unit cells at LT and HP were induced by the positional modulation of the $[NO_3]^-$. For the $[C_2mim][PFBS]$, the molecular orientational orders and molecular conformations of the $[PFBS]^-$ contributed to the large unit cell. No g' conformer of the $[PFBS]^-$, as indicated by the Raman spectrum shown in Fig. 3, was observed in the above unit cell. From the crystal structure analysis, the conformation ratio of t:g = 1:1 was obtained (Fig. 5(a)). Conversely, the Raman spectrum of the C_{II} phase suggests that t:g = 2:1 at 240 K (Fig. 3). The population discrepancy between the X-ray diffraction and Raman spectroscopy was due to the difficulty to determine the molecular conformations using X-ray diffraction.

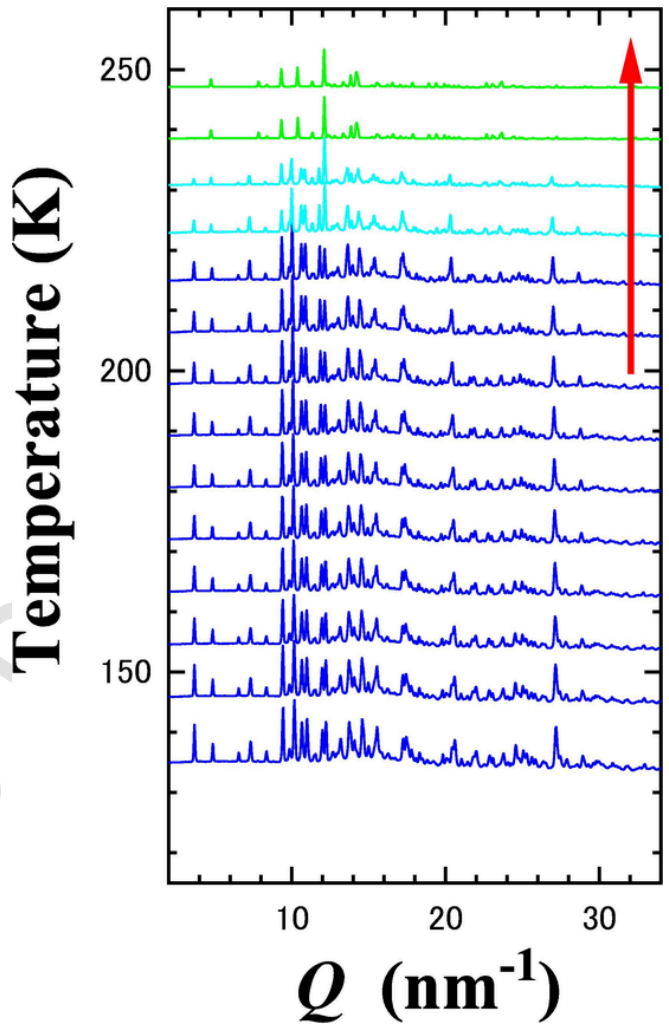

Fig. 4. X-ray diffraction patterns of the $[C_2mim][PFBS]$ upon heating using synchrotron radiation.

Table 1
Crystallographic data at low temperatures. *a*, *b*, *c*, α, β, and γ are the lattice parameters in the unit cell. *Z* is the number of cation–anion pairs in the unit cell. $_wR$ and *R* indicate the weighted reliability factor and reliability factor, respectively.

	Space group	*a* (nm)	*b* (nm)	*c* (nm)	α (°)	β (°)	γ (°)	*Z*	ρ (g/cm^3)	R_w (%)	*R* (%)
C_{II}	$P2_1/c$	1.0084	1.2393	2.6457	90	90.31	90	8	1.648	6.38	7.91
C_{III}	$P\bar{1}$	0.9707	1.7067	2.0152	90.15	81.64	87.59	8	1.651	5.76	6.06

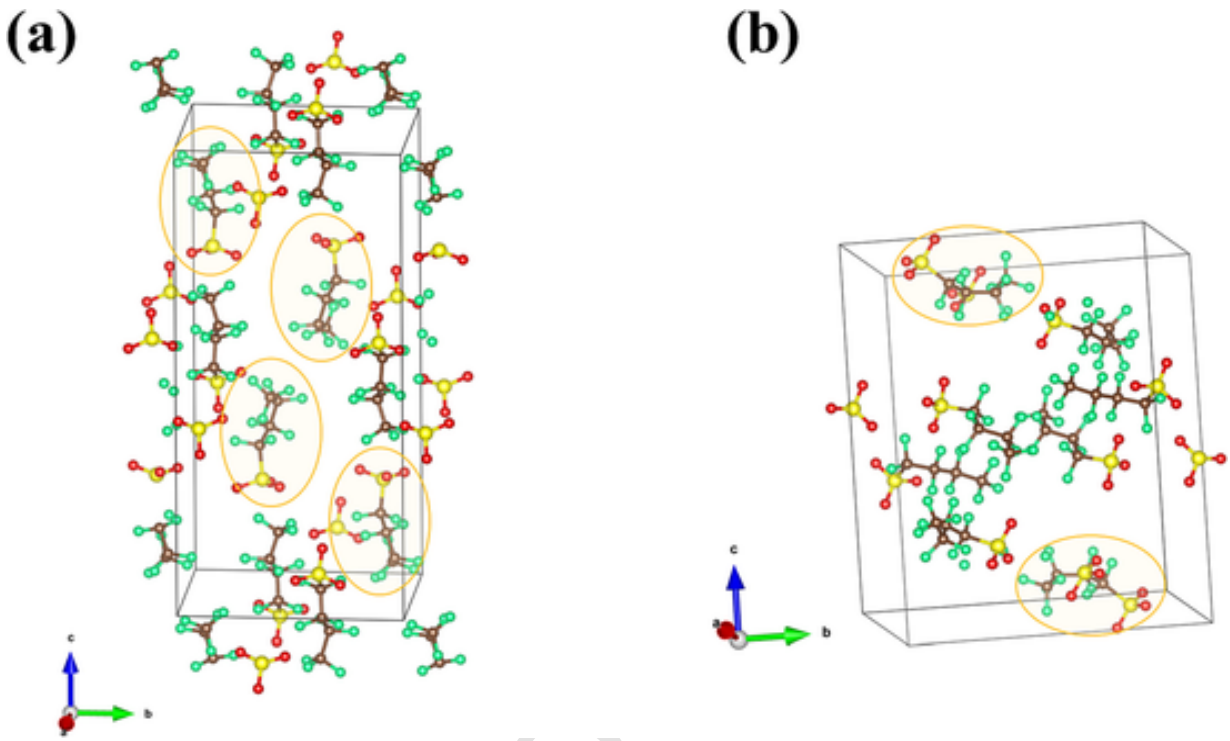

Fig. 5. Unit cells of the (a) C_{II} phase ($P2_1/c$) at 246.7 K and the (b) C_{III} phase ($P\bar{1}$) at 131.4 K. The g conformers in the unit cells are expressed by the orange circles.

The X-ray diffraction pattern of the C_{III} phase at 131 K was entirely different from that of the C_{II} phase (Fig. 4). The characteristic feature of the C_{III} phase was that the lowest Q peak appeared at 3.66 nm^{-1}. The lowest peak of the C_{III} phase did not exist in the C_{II} phase. Another point is that the 00ℓ Bragg reflections representing the layered structure in the HP $[C_6mim][PFBS]$ [20] were not observed in the C_{III} phase. From the X-ray diffraction pattern at 131 K, the crystal structure of the C_{III} phase having the large unit cell was determined to be triclinic (Table 1). The $[PFBS]^-$ molecules in the unit cell are displayed in Fig. 5(b), where the omitted $[C_2mim]^+$ conformers are NP. In the unit cell, the $[PFBS]^-$ conformational ratio was found to be t:g = 3:1. Considering that t:g = 4:1 using Raman spectroscopy at 125 K (Fig. 3), the conformational ratio in the unit cell had a discrepancy in the same manner as the C_{II} phase. However, the relative changes in the conformational ratios between the C_{II} and C_{III} phases were explained qualitatively by the structure analysis. The g conformers decreased in the C_{III} phase because of relatively high molecular packing.

4. Conclusions

The LT crystal polymorph of the $[C_2mim][PFBS]$ was clarified by X-ray diffraction and Raman spectroscopy. The LT phases were attributed to the molecular orientational orders and conformations, which contributed to the large unit cells. The C_{III} crystal structure of the well-packed phase was attributed to the small amount of the g and g' conformers of the $[PFBS]^-$ with relatively high molecular packing. The ideal and reversible crystal polymorph of the $[C_2mim][PFBS]$ was realized at LT.

CRediT authorship contribution statement

Hiroshi Abe : Conceptualization, Writing – original draft, Writing – review & editing. **Hiroaki Kishimura :** Data curation. **Mikio Uruichi :** Data curation. **Hajime Sagayama :** Data curation.

Declaration of Competing Interest

The authors declare that they have no known competing financial interests or personal relationships that could have appeared to influence the work reported in this paper.

Data availability

Data will be made available on request.

Acknowledgments

We thank Dr. T. Takekiyo and Prof. Y. Yoshimura of National Defense Academy for helpful discussion. We also appreciate Dr. S. Shimono of the National Defense Academy for experimental support. We acknowledge the support of Photon Factory (Proposal No. 2020G598). Crystal structures were displayed using *VESTA* 3 [32].

Appendix A. Supplementary material

Supplementary data to this article can be found online at https://doi.org/10.1016/j.chemphys.2023.112063.

References

[1] P.G. Debenedetti, F.H. Stillinger, Supercooled liquids and the glass transition, Nature 410 (2001) 259–267.
[2] K.M. Steed, J.W. Steed, Packing problems: high Z' crystal structures and their relationship to cocrystals, inclusion compounds, and polymorphism, Chem. Rev. 115 (2015) 2895–2933.
[3] A.J. Cruz-Cabeza, J. Bernstein, Conformational polymorphism, Chem. Rev. 114 (2014) 2170–2191.
[4] A. Johnston, A.J. Florence, N. Shankland, A.R. Kennedy, K. Shankland, S.L. Price, Crystallization and crystal energy landscape of hydrochlorothiazide, Cryst. Growth Des. 7 (2007) 705–712.
[5] S.L. Price, Why don't we find more polymorphs? Acta Cryst. B 69 (2013) 313–328.
[6] M.A. Neumann, J. van de Streek, F.P.A. Fabbiani, P. Hidber, O. Grassmann,

Combined crystal structure prediction and high-pressure crystallization in rational pharmaceutical polymorph screening, Nat. Commun. 6 (2015) 7793–7797.
[7] Z. Lei, B. Chen, Y.-M. Koo, D.R. MacFarlane, Introduction: ionic liquids, Chem. Rev. 117 (2017) 6633–6635.
[8] S. Zhang, N. Sun, X. He, X. Lu, X. Zhang, Physical properties of ionic liquids: database and evaluation, J. Phys. Chem. Ref. Data 35 (2006) 1475–1517.
[9] H. Abe, H. Kishimura, T. Takekiyo, Y. Yoshimura, N. Hamaya, Non-equilibrium protic and aprotic ionic liquids: measuring the distance from the equilibrium state, J. Mol. Liq. 283 (2019) 196–207.
[10] H. Abe, H. Kishimura, T. Takekiyo, T. Hanasaki, Y. Yoshimura, N. Hamaya, Low-temperature and high-pressure phase changes of room temperature ionic liquids, J. Mol. Liq. 300 (2020) 112340–112349.
[11] H. Abe, Phase variety in ionic liquids: hydrogen bonding and molecular conformations, J. Mol. Liq. 332 (2021) 115189–1115127.
[12] H. Abe, S. Tsuzuki, S. Ozawa, Anion effects on amorphization and crystallization in room-temperature ionic liquids, Chem. Phys. Lett. 712 (2018) 30–33.
[13] Y. Yoshida, K. Muroi, A. Otsuka, G. Saito, M. Takahashi, T. Yoko, 1-Ethyl-3-methylimidazolium based ionic liquids containing cyano groups: synthesis, characterization, and crystal structure, Inorg. Chem. 43 (2004) 1458–1462.
[14] H. Abe, T. Takekiyo, Y. Yoshimura, N. Hamaya, S. Ozawa, Crystal polymorphs and multiple crystallization pathways of highly pressurized 1-ethyl-3-methylimidazolium nitrate, Aust. J. Chem. 72 (2019) 87–92.
[15] V. Štejfa, J. Rohlíc˘ek, C. C˘ervinka, Phase behaviour and heat capacities of selected 1-ethyl-3-methylimidazolium-based ionic liquids, J. Chem. Thermodyn. 142 (2020) 106020–10.
[16] V. Štejfa, J. Rohlíček, C. Červinka, Phase behaviour and heat capacities of selected 1-ethyl-3-methylimidazolium-based ionic liquids II, J. Chem. Thermodyn. 160 (2021) 106392–1106312.
[17] Y. Koyama, S. Shimono, H. Abe, K. Matsuishi, Crystal polymorphs in 1-alkyl-3-methylimidazolium perfluorobutanesulfonate ionic liquids, J. Mol. Liq. 317 (2020) 113908–1113907.
[18] F. Chen, T. You, Y. Yuan, C. Pei, X. Ren, Y. Huang, Z. Yu, X. Li, H. Zheng, Y. Pan, K. Yang, L. Wang, Pressure-induced structural transitions of a room temperature ionic liquid—1-ethyl-3-methylimidazolium chloride, J. Chem. Phys. 146 (2017) 094502–094510.
[19] Y. Koyama, S. Shimono, H. Kishimura, T. Takekiyo, Y. Yoshimura, H. Abe, K. Matsuishi, High-pressure crystal polymorphs in 1-butyl-3-methylimidazolium perfluorobutanesulfonate, J. Mol. Liq. 335 (2021) 116415–116417.
[20] H. Abe, Y. Koyama, S. Shimono, H. Kishimura, K. Matsuishi, High-pressure crystal polymorphs and multiple pathways in 1-hexyl-3-methylimidazolium perfluorobutanesulfonate ionic liquid, Chem. Phys. 557 (2022) 111479–1111477.
[21] J.N. Canongia Lopes, J. Deschamps, A.A.H. Pádua, Modeling Ionic Liquids Using a Systematic All-Atom Force Field, J. Phys. Chem. B 108 (2004) 2038–2047.
[22] H. Abe, Y. Koyama, T. Takekiyo, Y. Yoshimura, High-pressure conformational and crystal polymorphs in 1-hexyl-3-methylimidazolium perfluorobutanesulfonate ionic liquid, *submitted to Vib. Spectros.*
[23] T. Arii, A. Kishi, Y. Kobayashi, A new simultaneous apparatus for X-ray diffractometry and differential scanning calorimetry (XRD-DSC), Thermochim Acta 325 (1999) 151–156.
[24] R. Oishi-Tomiyasu, Robust powder auto-indexing using many peaks, J. Appl. Cryst. 47 (2014) 593–598.
[25] V. Favre-Nicolin, R. C Ï erny, FOX, 'free objects for crystallography': a modular approach to *ab initio* structure determination from powder diffraction, J. Appl. Cryst. 35 (2002) 734–743.
[26] H. Abe, H. Kishimura, M. Uruichi, A phase variety of fluorinated ionic liquids: Molecular conformational and crystal polymorph, Spectrochim. Acta A 286 (2023) 121948–1121947.
[27] Y. Umebayashi, T. Fujimori, T. Sukizaki, M. Asada, K. Fujii, R. Kanzaki, S. Ishiguro, Evidence of conformational equilibrium of 1-ethyl-3-methylimidazolium in its ionic liquid salts: Raman spectroscopic study and quantum chemical calculations, Chem. A Eur. J. 109 (2005) 8976–8982.
[28] J.S. Wilkes, M.J. Zaworotko, Air and water stable I-ethyl-3-methylimidazolium based ionic liquids, J. Chem. Soc. Chem. Commun. 965–967 (1992).
[29] K. Matsumoto, R. Hagiwara, Z. Mazej, P. Benki˘c, B. Žemva, Crystal structures of frozen room temperature ionic liquids, 1-ethyl-3-methylimidazolium tetrafluoroborate ($EMImBF_4$), hexafluoroniobate ($EMImNbF_6$) and hexafluorotantalate ($EMImTaF_6$), determined by low-temperature X-ray diffraction, Solid State Sci. 8 (2006) 1250–1257.
[30] Y. Yoshimura, T. Takekiyo, H. Abe, N. Hamaya, High-pressure phase behavior of the room temperature ionic liquid 1-ethyl-3-methylimidazolium nitrate, J. Mol. Liq. 206 (2015) 89–94.
[31] N.S.M. Vieira, P.M. Reis, K. Shimizu, O.A. Cortes, I.M. Marrucho, J.M.M. Aráujo, J.M.S.S. Esperança, J.N. Canongia Lopes, A.B. Pereiro, L.P.N. Rebelo, A thermophysical and structural characterization of ionic liquids with alkyl and perfluoroalkyl side chains, RSC Adv. 5 (2015) 65337–65350.
[32] K. Momma, F. Izumi, VESTA 3 for three-dimensional visualization of crystal, volumetric and morphology data, J. Appl. Cryst. 44 (2011) 1272–1276.